WILDFIRE DETECTION USING STREAMING SATELLITE IMAGERY

Steven G. Xu, Seunghyun Kong, Zohreh Asgharzadeh

SAS Institute Inc.
Cary, North Carolina, 27513 USA
Steven.Xu@sas.com, Seunghyun.Kong@sas.com, Zohreh.Asgharzadeh@sas.com

ABSTRACT

We propose a novel wildfire detection algorithm for multispectral satellite images. By observing that wildfire pixels are sparse outliers residing in a spatially correlated background, we isolate them using robust principal component analysis. A novel cloud masking approach based on T-point thresholding is also proposed to reduce false alarms. Compared to existing methods, our proposed method adapts to the spatial and temporal heterogeneity of satellite images, does not require training on labeled images, and is computationally efficient for online monitoring. We present an application of our proposed algorithm to the GOES-R imagery in monitoring recent California wildfires.

***Index Terms*—** Unsupervised learning, RPCA, wildfire detection, multispectral imagery, image thresholding

1. INTRODUCTION

Uncontrolled wildfires can bring irreversible damage to both human communities and the environment. At a local scale, they pose serious threats to valuable assets and human safety; at a global scale, they precede emission of greenhouse gas and particles that negatively impact Earth's climate and public health. Despite various efforts, prevention of unexpected wildfires remains infeasible. Thus, detection and monitoring of wildfires have become paramount objectives in minimizing the economic and environmental costs. Early detection of wildfires ensures that suppression personnel can arrive on the scene timely, whereas real-time monitoring provides valuable information on the status change of active wildfires.

Current notification of active wildfires still relies heavily on human spotter reports whose effectiveness are limited to daytime wildfires in populated areas. To overcome these limitations, remote detection of wildfires using satellite imagery has been considered [1]. Most of the existing methods use Earth-orbiting satellite imagery for its high spatial resolution, but its low temporal resolution renders continuous monitoring of a wildfire impossible. Geostationary satellite imagery, although suitable for monitoring task, received little attention because its spatial resolution was considered too coarse to be useful. In recent years, the spatial resolution of geostationary satellite imagery has increased significantly. The Geostationary Operational Environmental Satellites (GOES)-16 [2], launched in 2017, is one of the newest weather satellites operated by NASA and the National Oceanic and Atmospheric Administration (NOAA) to provide high frequency Earth imagery and atmospheric measurements. It scans the continental U.S. (CONUS) every 5 minutes through 16 spectral bands covering visible and infrared wavelengths. The 2 km spatial resolution and high temporal resolution of GOES-16 imagery makes it suitable for detecting wildfires online.

Detecting wildfire using a satellite image is equivalent to classifying each pixel on the image as either non-fire or fire. The 3.9 μm band on GOES-16 in sensitive to subpixel heat, but detection based on 3.9 μm band only results in an overly sensitive algorithm that misclassifies warm background and reflective objects (e.g. cloud) as fire. To remedy, one can use both 3.9 μm and 12.3 μm bands of which the latter senses the actual near-ground temperature. A fire pixel can be identified by observing a significant and steady difference between brightness temperatures (BT) measured at these two bands.

A limited number of work on detecting wildfire based on GOES imagery has been proposed. The reference [3] uses fixed and contextually varying thresholding mechanisms on combinations of infrared bands to mask out cloud and detect fire pixels based on GOES-11/12 imagery. Its method requires setting a large number of threshold values which often need to be separately optimized for different scenarios; studies have also shown that its algorithm greedily focuses on recall rate and suffers from high false alarm rates. The reference [4] builds a deep convolutional neural net that utilizes spatial and spectral dependency structure of GOES-16 imagery to detect wildfire at pixel level, but does not explicitly mask out clouds and requires training over a large sample of labeled images. To date, an unsupervised online algorithm that simultaneously masks out cloud and detects wildfire pixels remains missing.

In this paper, a novel method to detect wildfires online based on GOES-16 imagery is introduced. Our detection is primarily based on BT difference between 3.9 μm and 12.3 μm bands. By observing that wildfire pixels are sparse outliers and background pixels are spatially correlated, we

propose to decompose the infrared image matrix, whose entries contain pixel-level BT differences, into low-rank and sparse components using robust principal component analysis (RPCA). To reduce false alarms due to cloud pixels, we also propose a novel cloud masking approach using histogram-based thresholding. Compared to existing methods, our algorithm is not optimized for individual scenario and is robust to variation in global environment. Our algorithm is also fully unsupervised and can perform online detection from a cold-start. Our experimental results on recent California wildfires show that our algorithm achieves timely detection with low false alarm rate.

2. METHODS

For an m by n GOES-16 image, let $\mathbf{Y}$ denote the data matrix containing BT difference between 3.9 μm and 12.3 μm bands. Potential wildfire pixels are outliers because of their intense response in BT difference, whereas background pixels are spatially correlated since adjacent pixels describe similar characteristics. Therefore, we can assume $\mathbf{Y}$ is the superposition of a sparse matrix $\mathbf{S}$ that contains potential wildfire pixels and a low-rank matrix $\mathbf{L}$ that contains the background pixels; i.e., $\mathbf{Y} = \mathbf{L} + \mathbf{S}$ (see Fig. 1 for an illustration). Under this assumption, identifying wildfire pixels in $\mathbf{Y}$ is equivalent to classifying nonzero entries in $\mathbf{S}$. Analogously, let $\mathbf{Y}_t,\ t = 1, 2, ...$ be the constructed data matrices for a stream of GOES-16 images. Then wildfire monitoring is equivalent to classifying nonzero entries in the corresponding sequence of sparse components $\mathbf{S}_t,\ t = 1, 2, ...$

2.1. Robust Principle Component Analysis

The sparse component $\mathbf{S}$ can be recovered by RPCA [5] through a two-objective optimization problem,

$$\min_{\mathbf{L},\mathbf{S}} \|\mathbf{L}\|_* + \lambda\|\mathbf{S}\|_1 \ s.t.\ \mathbf{Y} = \mathbf{L} + \mathbf{S} \tag{1}$$

where $\|\mathbf{L}\|_*$ is the sum of eigenvalues $\sum_i \sigma_i(\mathbf{L})$, and $\|\mathbf{S}\|_1$ is the ℓ_1-norm. The penalty coefficient λ controls the sparsity of $\mathbf{S}$. It has been proved that under surprisingly broad conditions, the choice of penalty coefficient $\lambda = \frac{1}{\sqrt{\max(m,n)}}$ can exactly recover the low-rank and sparse components [5].

2.2. Cloud Masking Using T-point Thresholding

The potential wildfire pixels in $\mathbf{S}$ often contain cloud pixels which are also characterized by high BT differences. To ensure our algorithm does not misclassify cloud as wildfire, we propose to identify a pixel in $\mathbf{S}$ as a cloud pixdel if its radiance at the 12.3 μm band, $R_{12.3}$, is significantly low. Water vapor absorbs atmospheric energy at 12.3 μm, therefore clouds are significantly cooler than the background in the 12.3 μm band. However, what qualifies as "significantly low" does not have a straightforward criterion, since patterns of cloud can vary dramatically across different scenarios. Therefore, a cloud masking mechanism that accounts for spatial and temporal variations should be employed. Consider the histogram of $R_{12.3}$; we expect it to be approximately unimodal, with a major peak at high radiance representing the background as the main population and a heavy lower tail representing the cloud pixels with substantially lower radiance. Therefore, cloud pixels can be masked out by finding the cutoff value that well separates the lower tail and bulk of the $R_{12.3}$ histogram.

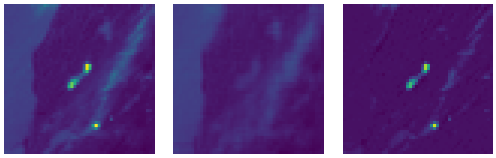

(a) $\mathbf{Y}$ (b) $\mathbf{L}$ (c) $\mathbf{S}$

Fig. 1: Decomposition of a BT difference image into low-rank and sparse components. (a) The original image. (b) The low-rank component containing spatially correlated background pixels. (c) The sparse component containing potential wildfire pixels.

The T-point algorithm [6] is an automatic image thresholding method based on the pixel density function. It assumes that the pixel density can be approximated by a unimodal histogram with a heavy upper tail. The histogram can be decomposed into three parts: a steep rising slope, a steep descending slope, and a slow descending slope. It then fits a piece-wise linear regression to the steep descending and the low descending slope. The optimal cutoff value is set equivalent to the knot that minimizes the fitting error, such as the ℓ_d-norm, $d \in \{1, 2\}$, of the regression. To see how the T-point algorithm can be used to mask out cloud pixels, let $\mathbf{r}$ denote a vector that stores the sorted negative pixel $R_{12.3}$ of an m by n image in ascending order. If cloud pixels contribute to the lower tail of the $R_{12.3}$ density, then they will contribute to the higher tail of the $-R_{12.3}$ density. Let $\mathbf{r}_{(i)},\ i \in [1, mn]$ be the $-R_{12.3}$ of the i-th entry. If we assume the peak of $-R_{12.3}$ histogram has been identified at index p, then the optimal cutoff index $t \in [p+1, mn-1]$ is found by solving the optimization problem

$$t = \arg\min \left\{ \sum_{i=p}^{t} \left|\mathbf{r}_{(i)} - \hat{\mathbf{r}}_{(i)}\right|^d + \sum_{i=t}^{mn} \left|\mathbf{r}_{(i)} - \hat{\mathbf{r}}_{(i)}\right|^d \right\} \tag{2}$$

where $\hat{\mathbf{r}}$ are the estimated $-R_{12.3}$ by the fitted regression lines. Following Equation (2), we will identify a pixel as wildfire only if its $R_{12.3}$ is above $-\mathbf{r}_{(t)}$. A visual illustration of cloud masking using T-point thresholding is shown in Fig. 2.

2.3. Noise Reduction

The potential wildfire pixels in $\mathbf{S}$ can also contain noise, which are often the results of a warm background that emits

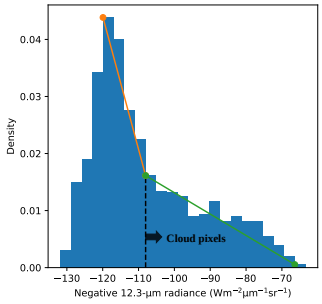

Fig. 2: Cloud masking based on T-point thresholding. The histogram of negative pixel radiance, the fitted piecewise regression lines as well as the optimal cutoff value are visualized.

terrestrial radiation and reflects solar radiation during the daytime. A low-pass filter is suitable for attenuating high-frequency noise while retaining the low-frequency signal. In this paper, we apply Gaussian smoothing to $\mathbf{S}$ and classify a pixel as a wildfire pixel only if its BT is above ΔK. We found in our experiments that $5 \leq \Delta K \leq 8$ achieves a reasonable balance between high sensitivity and specificity.

2.4. Grace Period

Our experimental results, presented in the next section, demonstrate the effectiveness of the proposed post-processing techniques across a broad setting. However, in case the false alarm rate needs to be further reduced, one can take advantage of the high temporal resolution of GOES-16 imagery and employ a grace period technique. That is, nonzero entries in $\mathbf{S}_t$ are identified as wildfire pixels only if they remain nonzero in the subsequent sparse components $\mathbf{S}_{t+1}, ..., \mathbf{S}_{t+L}$ where the length of the grace period L can be set according to the desired degree of sensitivity.

3. PRELIMINARY RESULTS

In this section, we provide some preliminary results of using the proposed algorithm to detect and monitor recent California wildfires. It is important to mention that not all wildfires are visible to GOES-16. This is because the infrared sensor equipped on GOES-16 has a resolution of 2 km, which can overlook fires with a burned size less than 4 km^2 (approximately 988 acres). In this paper, we focus on two visible ones: the Kincade fire and the Walker fire (Information is available on `https://www.fire.ca.gov/incidents/2019/`).

3.1. Kincade Fire

The Kincade fire started on October 23, 2019. It burned an area of 77,758 acres before fully contained on November 6, 2019. Image data spanning the full 24-hour period of October 28 with a total of 288 frames were downloaded. The fire was visible to GOES-16 in all frames. A 100 km $\times$ 100 km region in Northern California was cropped from the original CONUS region for analysis. Besides the Kincade Fire, a second cluster of pixels with persistently high BT difference was spotted during the analysis; it was later confirmed to be the Grizzly Island fire which was also active on October 28. RPCA was applied to each frame to recover the corresponding sparse components. The cloud pixels are masked out using the T-point method; the noise pixels are removed using Gaussian smoothing and fixed thresholding with $\Delta K = 6$. Visualized results of three frames uniformly sampled from the 24 hour period are shown in Fig. 3 (a)–(c). Our proposed method detects both the Kincade fire and the Grizzly Island fire in all three frames with low false alarm rates.

3.2. Walker Fire

The Walker fire started on September 4, 2019. It was initially estimated to have a maximum size of 5 acres but later grew significantly because of strong and erratic winds. It eventually burned up to 54,612 acres before fully contained on September 25, 2019. Image data spanning the full 24-hour period of September 5 were downloaded. The size of the Walker fire was initially too small to be visible until the evening of September 5. Therefore, the fire is detectable only in the later half of the downloaded frames. A 100 km $\times$ 100 km region in Northern California is again cropped as the training frame size, and wildfire detection is applied using the same pipelines described in Section 3.1. Visualized results of three frames uniformly sampled from the 24 hour period are shown in Fig. 3 (d)–(f). The first frame was captured when the Walker fire was still invisible and therefore no wildfire pixel can be detected. In the remaining two frames where the Walker Fire was visible to GOES-16, our algorithm successfully detects it in both frames. Furthermore, not a single false alarm was raised even though large coverage of cloud exists in all three frames.

As emphasized throughout the paper, the proposed method can also be used to monitor formation or status change of wildfire in a real-time image stream. To demonstrate the proposed method's effectiveness in capturing the Walker fire's size change on September 5, we monitor the 288 frames assuming they are received in an online setting. The result on a sample of six consecutive frames is shown in Fig. 3 (g)–(l). These frames cover a short time range in which the Walker Fire transitioned from undetectable to detectable. We see that actual wildfire pixels are identified as early as 8:23 pm. However, false alarms are detected at 8:13 pm, 8:18 pm and 8:28 pm. As mentioned in Section 2.4, the specificity of the proposed detection algorithm can be further improved by using a grace period technique. If we apply a grace period of length 1 ($L = 1$) to the frames in Fig. 3 (g)–(l), then potential fire pixels at 8:13 pm, 8:18 pm and 8:28 pm will not be flagged as actual fire pixels since

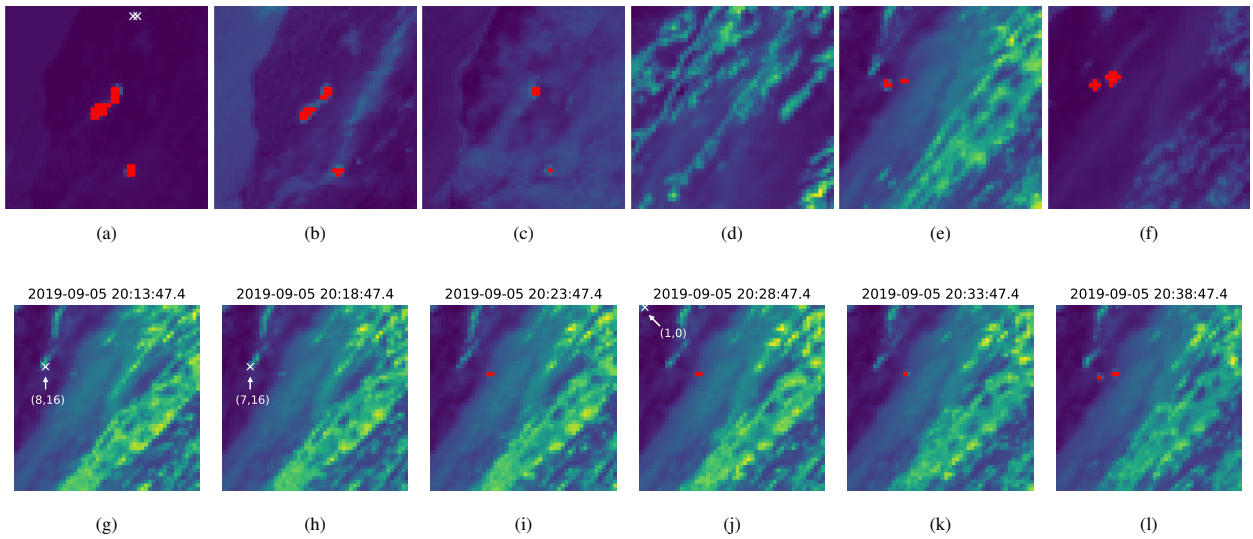

Fig. 3: Experimental Results. First row: frame-wise detection of the Kincade fire and Grizzly Island fire (a)–(c), and the Walker Fire (d)–(f). Second row: monitoring the Walker fire online. In each figure, red dots represent correctly identified wildfire pixels and white crosses represent false alarms. In monitoring results only, the (x, y) location of each false alarm, with $(0, 0)$ representing the left top corner, is also shown.

they were not detected in the subsequent frames. As a result, we will be able to confirm our detection of the Walker fire at 8:28 pm without making any false alarms. According to online report (`https://www.plumasnews.com/walker-fire-day-3-updates`), the approximate time when the size of Walker fire became detectable by GOES-16 is between 7:25 pm and 8:55 pm, which is reasonably close to our result.

Our experiment can be improved by including comparison with existing methods that are also designed for GOES imagery. One particular challenge is finding a suitable metric for numerical comparison, since the limitation of GEOS imagery's spatial resolution and absence of ground truth make locating the exact wildfire coordinates and validating the detection accuracy extremely difficult. Furthermore, comparison to methods designed for other satellite instruments (e.g. MODIS) is also possible. We will propose these extension in near future.

4. CONCLUSION

In this paper, we proposed an unsupervised wildfire detection algorithm for GOES-16 images using RPCA. A novel cloud masking approach based on T-point thresholding is also proposed to reduce false alarms. Our algorithm adapts to the spatial and temporal heterogeneity of satellite images, does not require training on labeled images, and is computationally efficient enough for online monitoring. Experimental results on varying scenarios demonstrated that our algorithm can detect wildfires accurately and timely. It should be noted that although this paper focused on GOES-16 imagery, our algorithm can be applied to imagery obtained from other satellite instruments after trivial modifications.

5. REFERENCES

[1] Panagiotis Barmpoutis, Periklis Papaioannou, Kosmas Dimitropoulos, and Nikos Grammalidis, "A review on early forest fire detection systems using optical remote sensing," *Sensors*, vol. 20, no. 22, pp. 6442, 2020.

[2] *Geostationary Operational Environmental Satellites - R Series, A collaborative NOAA & NASA program. Jul. 2012*.

[3] W Xu, MJ Wooster, G Roberts, and P Freeborn, "New GOES imager algorithms for cloud and active fire detection and fire radiative power assessment across North, South and Central America," *Remote Sensing of Environment*, vol. 114, no. 9, pp. 1876–1895, 2010.

[4] Thanh Cong Phan and Thanh Tam Nguyen, "Remote sensing meets deep learning: Exploiting spatio-temporal-spectral satellite images for early wildfire detection," Tech. Rep., 2019.

[5] Emmanuel J Candès, Xiaodong Li, Yi Ma, and John Wright, "Robust principal component analysis?," *Journal of the ACM (JACM)*, vol. 58, no. 3, pp. 1–37, 2011.

[6] Nicolas Coudray, Jean-Luc Buessler, and Jean-Philippe Urban, "Robust threshold estimation for images with unimodal histograms," *Pattern Recognition Letters*, vol. 31, no. 9, pp. 1010–1019, 2010.